Journal of Electronics and Information Science (2025)
Clausius Scientific Press, Canada

DOI: 10.23977/jeis.2025.100103
ISSN 2371-9524 Vol. 10 Num. 1

Synchronous detection system for temperature and strain in partial discharges of three-phase cables based on FBG and neural networks

Gaopeng Zhang[a], Yao Zhao[b,*]

School of Physics and Electronic Information Engineering, Henan Polytechnic University, Jiaozuo, 454000, China
[a]13148272629@163.com, [b]zhaoyao@hpu.edu.cn
**Corresponding author*

Keywords: Fiber Bragg grating, Back Propagation Neural Network, Partial Discharge fault

Abstract: To detect the partial discharge (PD) faults in three-phase cross-linked polyethylene (XLPE) cable joints, this paper designs a parallel sensing detection system based on fiber Bragg gratings (FBG). By measuring the changes in the reflected power of FBGs in each branch and combining with a Back Propagation (BP) neural network algorithm, the demodulation of temperature and strain during PD is achieved. To verify the feasibility of this system, vibration signals and temperature changes are respectively applied to each FBG, and simulation experiments are carried out. The experimental results show that this system can accurately detect the temperature changes, the frequencies of vibration signals, and the strains in each branch, verifying its feasibility for detecting cable joint faults. In addition, by adjusting the sampling frequency of the photodetector, higher-frequency vibration signals can be measured.

1. Introduction

In recent years, the advancement of technology and the acceleration of urbanization have promoted the popularization of smart home appliances and new-energy vehicles, leading to a sharp increase in the public's electricity demand. Three-phase cross-linked polyethylene (XLPE) cables, characterized by their low dielectric loss, ease of manufacture, corrosion resistance, flexibility, and environmental friendliness[1,2], have found widespread application in power transmission[3-7]. However, due to the prolonged exposure of cables to complex underground environments, moisture and microorganisms in the soil can degrade the insulation layer of the cables, leading to partial discharge (PD) phenomena. Through long-term monitoring of operating cables, researchers have discovered that cable joints are high-incidence areas for PD[8,9]. Prolonged discharge activity can result in the formation of electrical treeing[10], which is accompanied by significant energy changes, including temperature, strain, and vibration. Ultimately, this can lead to complete destruction of the cable's insulation layer, causing power transmission interruptions and even serious safety accidents. Therefore, the development of efficient, intelligent, and low-cost underground cable fault monitoring systems is of great significance for maintaining the stable operation of power

systems[11].

Fiber Bragg Grating (FBG) sensors have received considerable attention in fault detection due to their high sensitivity to physical parameters such as temperature and strain[12-17]. Her.SC et al. [18] employed two FBGs with different center wavelengths, adhering one FBG to the main body of the structure while keeping the other in a free state. By measuring the Bragg wavelength shifts of the FBGs, they achieved simultaneous measurement of temperature and strain. Sarkar.S et al.[19] utilized a machine learning approach to construct a network model, enabling simultaneous demodulation of temperature and strain effects from a single measurement of FBG center wavelength changes. Experimental results demonstrated that the model achieved an accuracy of 90% in predicting both strain and temperature. Existing research methods typically rely on spectrometers to measure the central wavelength shift of FBGs for detecting changes in temperature and strain. However, these methods are often characterized by complex demodulation equipment and limited accuracy. Alternatively, measuring the variation in reflected power of FBGs can effectively address these issues. As indicated in references[20,21], the reflected power of an FBG can be calculated as the product of its reflectivity and the optical power from the light source. When PD occurs at a cable joint, the resulting electrical spark causes an instantaneous increase in the temperature of the cable insulation layer, along with the generation of a vibration signal characterized by high frequency and low amplitude[22-28]. During fault detection using FBGs, vibration signals induce strain changes in the FBG, while the increase in the cable insulation temperature simultaneously causes a corresponding rise in the FBG temperature. These changes in both temperature and strain of the FBG alter the refractive index of the grating, resulting in a shift of the reflected wavelength towards longer wavelengths. This wavelength shift gradually reduces the overlap between the reflected spectrum of the FBG and the laser light source, leading to a decrease in the reflected power. Based on this principle, we have designed an FBG-based sensing and detection system for monitoring PD faults at three-phase XLPE cable joints. By measuring the variations in the FBG reflected power and processing the data using a one-input, two-output Backpropagation (BP) neural network model, both temperature and strain changes can be simultaneously derived, enabling the detection of PD faults at cable joints.

To validate the fault detection capability of the proposed sensing and detection system, we conducted simulation experiments using dedicated software, applying vibration signals and introducing temperature variations to the FBGs on each branch separately. Additionally, a BP neural network model was developed to process the reflected power measured from each branch. The experimental results demonstrate that the system can accurately measure the strain and temperature changes in the FBGs induced by PD, as well as accurately demodulate the frequency of the vibration signals applied to each FBG, thereby enabling fault detection and localization. These results demonstrate the effectiveness and practicality of the proposed measurement system and data processing method. Furthermore, compared to the traditional approach of using spectral analyzers to measure central wavelength shifts, the method presented in this study, which utilizes reflected power to simultaneously detect vibration signals and temperature changes, offers several advantages. It not only simplifies system configuration and operation, and reduces system complexity and maintenance costs, but also significantly improves the efficiency of data processing and analysis.

2. Simulation experiment

2.1. Experimental system and principle

A sensing and detection system based on FBG has been designed for detectting PD faults at the joints of three-phase XLPE cables, as shown in Figure 1. A narrow-band pulsed laser enters the optical circulator through port 1 and exits through port 2 into the optical fiber. The light then passes

through a 1×3 power splitter, which evenly distributes it in a ratio of 1:1:1 to three branches. FBG1, FBG2, and FBG3 are used to detect PD faults at the joints of phase A, phase B, and phase C of the three-phase XLPE cables, respectively.

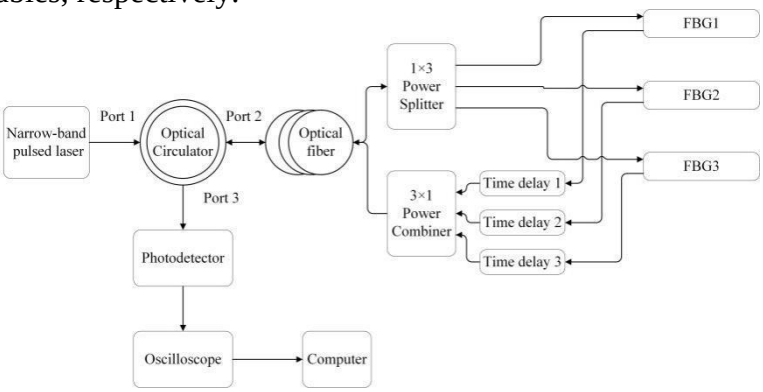

Figure 1: Experimental system structure diagram.

When PD occurs at cable joints, the temperature changes and vibration signals can induce corresponding variations in temperature and strain sensed by the FBGs, subsequently affecting the reflected power of the FBGs. To distinguish the reflected waveforms from the three FBGs across the three branches, the system employs Time-Division Multiplexing (TDM) technology to introduce distinct time delays for each FBG. Specifically, Time delay 1, Time delay 2, and Time delay 3 are set to 0 ns, 2 ns, and 4 ns, respectively. This configuration ensures that the reflected waveforms from all FBGs do not overlap in the time domain. The reflected light from each FBG is combined using a 3×1 power combiner and directed back into to the optical fiber. It then re-enters the optical circulator through port 2 and exits through port 3 to the photodetector. The photodetector converts the optical signal into an electrical signal, which is subsequently fed into the oscilloscope. As shown in Figure 2, the waveforms of the reflected power from the three FBGs can be observed on the oscilloscope. Finally, the reflected power variations from the three FBGs are measured using the oscilloscope for subsequent data processing, completing the demodulation of the vibration signals.

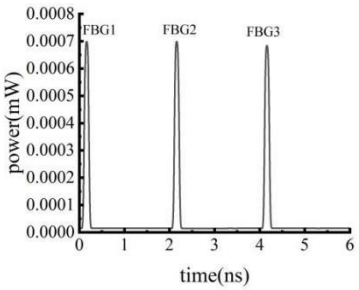

Figure 2: Reflected waveforms from three FBGs.

The center wavelength of the light source in the system is 1550 nm, with a spectral linewidth of 300 kHz and a peak pulse power of 50 mW. The insertion loss of the optical circulator is 0.7 dB. The length of the optical fiber is 0.2 km, with a loss of 0.04 dB. The loss of the 1×3 power splitter is 5.5 dB, and the loss of the 3×1 Power Combiner is also 5.5 dB. The three FBGs share the same specifications, with a center wavelength of 1550 nm, a bandwidth of 1 nm, and a reflectivity of 0.01. Additionally, this system can measure vibration signals of higher frequencies by adjusting the sampling frequency of the photodetector.

2.2. Experimental data measurement

Since XLPE cables can operate normally at temperatures up to 90 ℃[29-30], we conducted experiments to investigate the relationship between reflected power and temperature variations, as well as between reflected power and strain changes. The results indicate that the reflected power of the FBG gradually decreases as the temperature increases. Notably, within the temperature range of 100 ℃ to 110 ℃, a distinct linear relationship is observed between the reflected power and temperature. Similarly, within the strain range of 100 to 200 με, a clear linear relationship is also evident between reflected power and strain. Linear regression analysis revealed that the average sensitivity of the FBG sensor for temperature detection is 1.375×10^{-4} mW/℃, and the average sensitivity for strain detection is 1.448×10^{-5} mW/με.

To further investigate the variation in FBG reflected power when both strain and temperature changes occur simultaneously, we first set the temperature to 100 ℃ and measured 200 datasets as the strain increased in increments of 0.5 με, ranging from 100 με to 199.5 με. Subsequently, we conducted 19 additional experiments in which the temperature was incremented by 0.5 ℃, from 100°C to 109.5°C, while the strain varied within the range of 100 με to 199.5 με, also in increments of 0.5 με. In total, 4000 datasets were obtained. The measured changes in reflected power are illustrated in Figure 3.

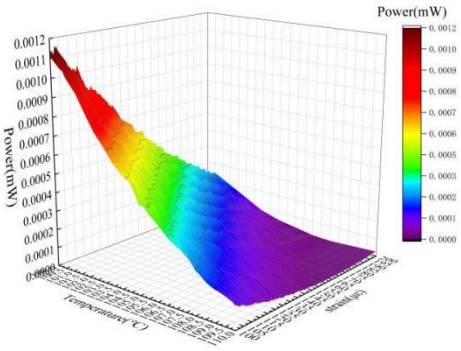

Figure 3: The variation in reflected power of FBG when influenced by both temperature and strain.

2.3. Data processing using BP neural networks

To simultaneously demodulate the strain and temperature changes induced during PD in cables using FBG reflected power variation data, we employ a BP neural network to construct a model with one input and two outputs, as shown in Figure 4. This model takes the reflected power of the FBG as the input and outputs the temperature change and the strain change caused by the PD, respectively. We denote the reflected power as P, and the temperature and strain of the FBG as T and S, respectively. Meanwhile, we have taken into account that the FBG sensors in the three branches of the system share the same configuration. Consequently, the one input and two output neural network model designed for one of the branches can also be used to process the data measured by the FBG sensors in the other two branches. This approach can significantly reduce the complexity of the model.

To improve the accuracy of model prediction, we performed several steps during the training process. First, we normalized the data, scaling its range between 0 and 1 to reduce the computational complexity of the model. Then, the data were randomly divided into training, validation, and test sets in a ratio of 8:1:1. The training and the validation sets were used for parameter adjustment. In addition, we employed the mini-batch gradient descent method and the K-fold cross-validation method. The mean squared error (MSE) loss function was employed for

model evaluation. After several rounds of parameter adjustment, in order to balance the training time and the accuracy of model prediction, we set the number of hidden layers *n* in the model to 5. The number of neuron nodes *m* in each layer was set to 8, 10, 15, 10, and 8 respectively. The mini-batch size was set to 10, K in K-fold cross-validation was set to 10, the number of training epochs was set to 5000, the learning rate was set to 0.0005, and the error threshold was set to 0.00005. After training, the model achieved an average prediction accuracy of 95.74% on the validation set. To evaluate the model's generalization performance, we fed the test set data into the trained model, achieving an average prediction accuracy of 95.36% on the test set.

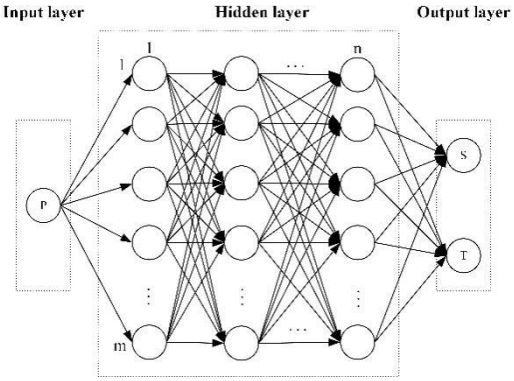

Figure 4: Structure diagram of designed BP neural network.

(a) (b)

Figure 5: Performance results on the validation set: (a) temperature; (b) strain.

To avoid data point overlap and better illustrate the model's predictive performance, we selected the 20 data points with the lowest prediction accuracy from both the validation and test sets for visualization, as shown in Figure 5 and Figure 6. The error between the predicted values of the model and the actual values remains at a low level.

(a) (b)

Figure 6: Performance results on the test set: (a) temperature; (b) strain.

3. Experimental result

Following the completion of model training, we conducted additional simulation experiments to validate the model's effectiveness. In these experiments, we applied simultaneous temperature and strain changes to the FBGs on three branches of the system and measured their reflected power.

Figure 7(a) displays the vibration signal applied to FBG1, which includes frequency components of 1000 Hz, 2000 Hz, 2100 Hz, 3000 Hz, and 4900 Hz. Figure 8(a) shows the vibration signal loaded onto FBG2, consisting of frequency components of 500 Hz, 1000 Hz, 2000 Hz, 3000 Hz, and 4000 Hz. Figure 9(a) presents the vibration signal applied to FBG3, with frequency components of 1000 Hz, 2000 Hz, 3000 Hz, 3500 Hz, and 4500 Hz. Collectively, these three sets of signals cover a frequency range from 0 to 5000 Hz, with strain magnitudes consistently falling within the interval of 100 to 200 με.

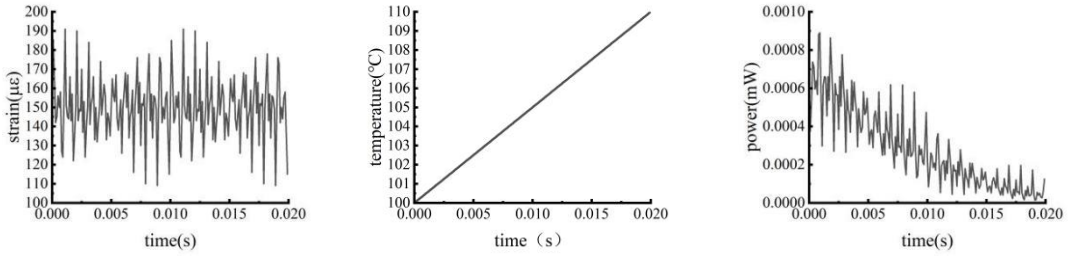

(a) (b) (c)

Figure 7: FBG1: (a) Strain applied to FBG1; (b) temperature applied to FBG1; (c) Reflected power of the FBG1.

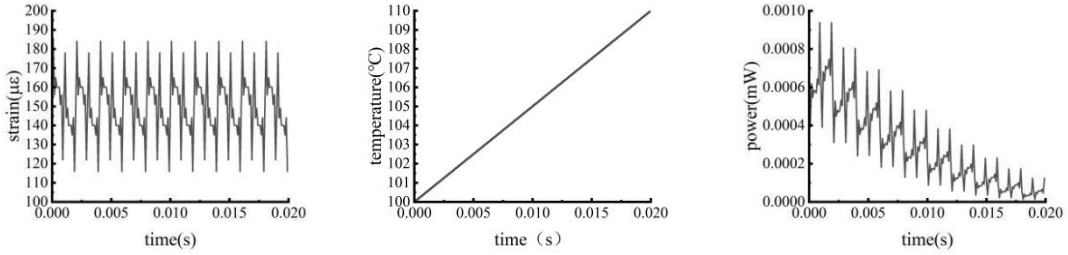

(a) (b) (c)

Figure 8: FBG2: (a) Strain applied to FBG2; (b) temperature applied to FBG2; (c) Reflected power of the FBG2.

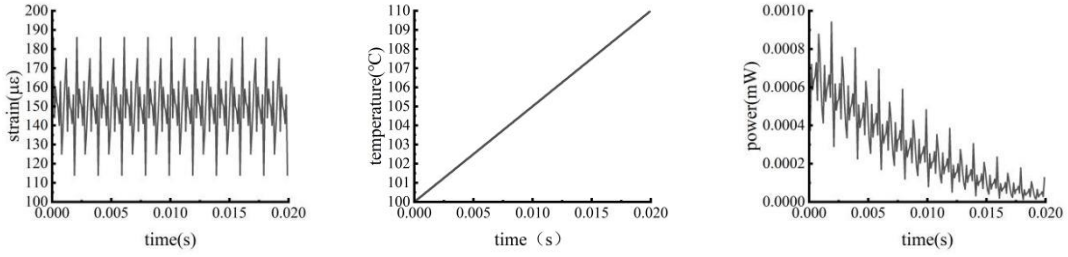

(a) (b) (c)

Figure 9: FBG3: (a) Strain applied to FBG3;(b) temperature applied to FBG3; (c) Reflected power of the FBG3.

Furthermore, due to the similar temperatures at the joints when PD occurs in three-phase cables, we set the temperature changes on all three branches to be consistent, as shown in Figures 7(b), 8(b), and 9(b). The temperature remained within the range of 100 to 110 ℃ throughout the experiments. Next, we measured the reflected power variation data for each FBG under the combined effects of vibration signals and temperature changes, as illustrated in Figures 7(c), 8(c), and 9(c). Using the trained model, we input the reflected power data on the three branches to predict the corresponding strain and temperature changes. These predicted values were then compared with the actual values used in the simulation experiments, as shown in Figures 10 and 11. Specifically, Figures 10(a), (b),

and (c) compare the predicted strain values with the actual strain values on the three branches, while Figures 11(a), (b), and (c) compare the predicted temperature values with the actual temperature values on the three branches.

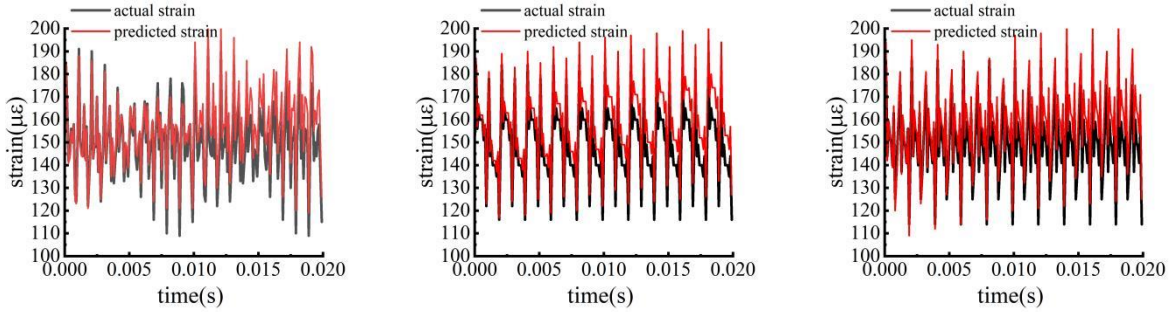

(a) (b) (c)

Figure 10: Comparison of the actual strain values and the strain values predicted: (a) FBG1;(b) FBG2; (c) FBG3.

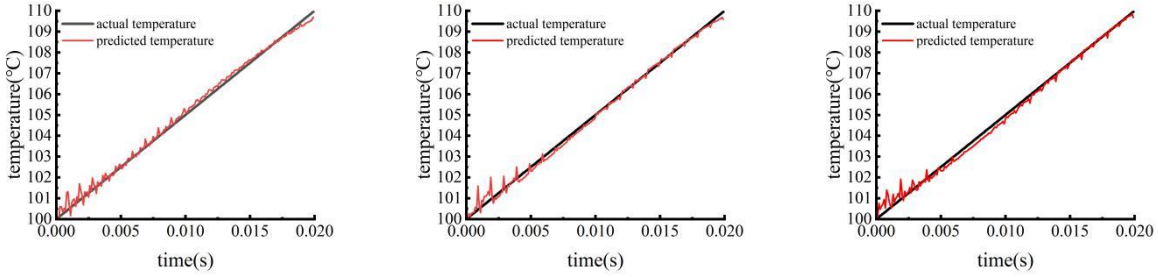

(a) (b) (c)

Figure 11: Comparison of the actual temperature values and the temperature values predicted: (a) FBG1;(b) FBG2; (c) FBG3.

As shown in Figures 10 and 11, the strains and temperatures predicted by the neural network model exhibit strong consistency with the strains and temperatures applied in the experiments. The average relative errors for the strain values of FBG1, FBG2, and FBG3 are 4.76%, 5.43%, and 5.50%, respectively. The average relative errors for the temperature values of FBG1, FBG2, and FBG3 are 0.15%, 0.14%, and 0.16%, respectively. These results confirm that the designed neural network model can accurately demodulate both temperature and strain changes. Subsequently, Fourier transform techniques were utilized to demodulate the frequency of the strain values predicted by the neural network model. The demodulated frequency values were then compared with the frequency values of the vibration signals applied in the experiments, as shown in Figure 12.

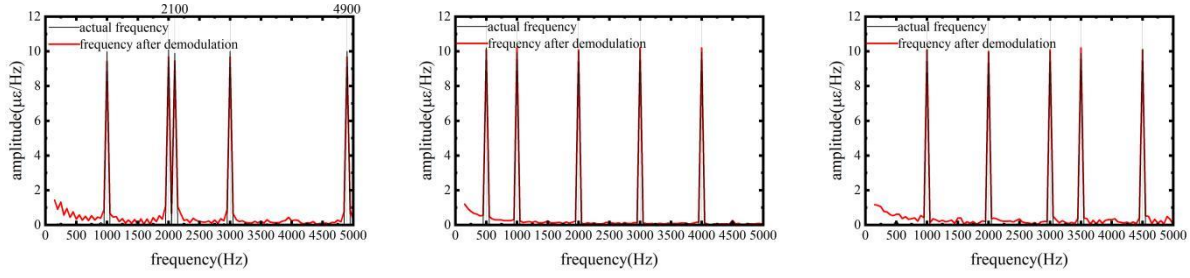

(a) (b) (c)

Figure 12: Comparison of the demodulated frequency values with those of the vibration signals applied during experiments: (a) FBG1; (b) FBG2; (c) FBG3.

As can be seen from Figures 12(a), (b), and (c), the demodulated frequency components are consistent with the frequency components of the vibration signals applied to each FBG during the experiments. These results demonstrate the feasibility of the proposed PD fault detection system and the method of simultaneously demodulating temperature and strain changes using the neural network algorithm.

4. Conclusions

In this paper, an FBG-based sensing system is designed, which comprises three parallel branches. The FBGs on these three branches are used for detecting PD faults at the phase A, phase B, and phase C joints of three-phase XLPE cables, respectively. To validate the effectiveness of the system, simulation experiments were conducted in which strain signals and temperature variations were simultaneously applied to the FBGs of the three branches. These experiments simulated the vibration signals and temperature changes resulting from PD, and the variations in the reflected power of the FBGs were measured. Subsequently, a BP neural network model was constructed for data processing. The experimental results indicate that the strains and temperatures predicted by the neural network are consistent with those actually applied to each FBG. Based on this, Fourier transform techniques were utilized to calculate the frequencies contained in the vibration signals applied to each FBG, which align with the frequency components of the vibration signals applied during the experiments. These results demonstrate the effectiveness and feasibility of the proposed PD fault detection system and data processing method. In addition, the system proposed in this paper is scalable. More FBG sensors can be connected in series in each branch, thereby expanding the detection range of PD faults. Moreover, the method used in this system to demodulate temperature and strain simultaneously using reflected power, compared with the traditional central wavelength demodulation method, significantly reduces system complexity and detection cost. In terms of data processing, the neural network model designed in this paper also supports the data processing of large-scale detection systems. Specifically, the one input and two output neural network model designed for one branch is equally applicable to processing the data detected by sensors in the other two branches. Compared with a multi-input and multi-output model that considers all FBG sensors of all branches in the system, the model constructed in this paper exhibits higher training efficiency and accuracy. In conclusion, the research findings of this paper provide a valuable reference solution for the large-scale detection of cable faults and are expected to be widely applied in the power industry.

Acknowledgments

This work was supported by the Doctoral Fund of Henan Polytechnic University (No. B2021-62, No. B2021-63).

References

[1] Gao C, He D, Zhou Y, et al. A Study on the Space Charge Characteristics of AC Sliced XLPE Cables[J]. IEEE Access, 2019, 7: 20531-20537.
[2] Katz C, Walker M, Fryszczyn B. Comparative Laboratory Evaluation of TR-XLPE and XLPE Cables With Super-Smooth Conductor Shields [J]. IEEE Transactions on Power Delivery, 2004, 19(4): 1532-1537.
[3] Morishita Y. Technical trends of high voltage and large capacity underground power cables[J]. IEEJ Transactions on Electrical and Electronic Engineering, 2007, 2(5): 531-535.
[4] Bak C L, Faria Da Silva F. High voltage AC underground cable systems for power transmission – A review of the Danish experience, part 1[J]. Electric Power Systems Research, 2016, 140: 984-994.
[5] Bak C L, Faria Da Silva F. High Voltage AC underground cable systems for power transmission – A review of the Danish experience: Part 2[J]. Electric Power Systems Research, 2016, 140: 995-1004.

[6] Wang J Q, Li W K, Zhang W Y, et al. Aging and life control of cross-linked polyethylene as cable insulation material [J]. Acta Physica Sinica, 2024, 73(7): 078801.
[7] Chen X, Yu J, Zhou H. Thermo-electric field analysis of AC XLPE cable in monopole, bipole, and tripole DC operation modes [J]. IET Generation, Transmission & Distribution, 2019, 13(14): 2959-2966.
[8] Kim K W, Kim Y K, Park D H. A Study on the Harmonics Current Detection and Comparison Analysis of High Pressure Cable Using Current Detection Sensor [J]. Journal of the Korean Institute of Illuminating and Electrical Installation Engineers, 2020, 34(9): 7-11.
[9] Toya A, Shimazu M, Umeda S, et al. Recent technologies of joints for HV and EHV XLPE cables in Japan [J]. IEEJ Transactions on Electrical and Electronic Engineering, 2007, 2(5): 523-530.
[10] Gao C, Yu Y, Wang Z, et al. Study on the Relationship between Electrical Tree Development and Partial Discharge of XLPE Cables[J]. Journal of Nanomaterials, 2019, 2019: 1-10.
[11] Winkelmann E, Shevchenko I, Steiner C, et al. Monitoring of Partial Discharges in HVDC Power Cables[J]. IEEE Electrical Insulation Magazine, 2022, 38(1): 7-18.
[12] Lee B. Review of the present status of optical fiber sensors[J]. Optical Fiber Technology, 2003, 9(2): 57-79.
[13] Majumder M, Gangopadhyay T K, Chakraborty A K, et al. Fiber Bragg gratings in structural health monitoring—Present status and applications[J]. Sensors and Actuators A: Physical, 2008, 147(1): 150-164.
[14] Mihailov S J. Fiber Bragg Grating Sensors for Harsh Environments [J]. Sensors, 2012, 12(2): 1898-1918.
[15] Xu S, Li X, Wang T, et al. Fiber Bragg grating pressure sensors: a review[J]. Optical Engineering, 2023, 62(01):010902.
[16] Hsiao T C, Hsieh T S, Chen Y C, et al. Metal-coated fiber Bragg grating for dynamic temperature sensor[J]. Optik, 2016, 127(22): 10740-10745.
[17] Singh A K, Berggren S, Zhu Y, et al. Simultaneous strain and temperature measurement using a single fiber Bragg grating embedded in a composite laminate[J]. Smart Materials and Structures, 2017, 26(11): 115025.
[18] Her S C, Lin W N. Simultaneous Measurement of Temperature and Mechanical Strain Using a Fiber Bragg Grating Sensor [J]. Sensors, 2020, 20(15): 4223.
[19] Sarkar S, Inupakutika D, Banerjee M, et al. Machine Learning Methods for Discriminating Strain and Temperature Effects on FBG-Based Sensors[J]. IEEE Photonics Technology Letters, 2021, 33(16): 876-879.
[20] Y uan L, Zhao Y, Sato S. Development of a low-cost and miniaturized fiber Bragg grating strain sensor system[J]. Japanese Journal of Applied Physics, 2017, 56(5): 052502.
[21] Atsushi Wada. Vibration sensing by using optical fiber Bragg gratings[J]. Acoustical Society of Japan, 2019: 663-668.
[22] Laili M S, Abdul Halim M H A, Arshad S N M, et al. Impact of Vibration Exciter on the Partial Discharge Characteristics in XLPE Cable[C]//2023 International Workshop on Artificial Intelligence and Image Processing (IWAIIP). IEEE, 2023: 321-324.
[23] Czaszejko T, Sookun J. Acoustic emission from partial discharges in cable termination[C]//Proceedings of 2014 International Symposium on Electrical Insulating Materials. IEEE, 2014: 42-45.
[24] Wu X, Li R, Ni H, et al. Integrated Detection of Temperature and Partial Discharge on Cables Based on FBG[C]//2019 2nd International Conference on Electrical Materials and Power Equipment (ICEMPE). IEEE, 2019: 385-389.
[25] Qifei Z, Bin M. Design of Partial Discharge Monitoring Algorithm for Transmission Cable Based on Optical Fiber Sensing Technology[C]//2023 International Conference on Power, Electrical Engineering, Electronics and Control (PEEEC). IEEE, 2023: 555-559.
[26] Fabris L V M, Silva J C C da. Simulation of Current Pulses and Sound Waves Resulting from Partial Discharges in a Needle-Plane Geometry in Air [J]. Journal of Microwaves, Optoelectronics and Electromagnetic Applications, 2022, 21(4): 481-507.
[27] Govindarajan S, Morales A, Ardila-rey J A, et al. A review on partial discharge diagnosis in cables: Theory, techniques, and trends [J]. Measurement, 2023, 216: 112882.
[28] Li Z, Wang H, Du B. Effect of Polycyclic Aromatic Compounds on Electrical Treeing Growth in XLPE Insulation[J]. IEEE Transactions on Dielectrics and Electrical Insulation, 2023, 30(1): 193-201.
[29] Chen X, Xu Y, Cao X, et al. Electrical treeing behavior at high temperature in XLPE cable insulation samples [J]. IEEE Transactions on Dielectrics and Electrical Insulation, 2015, 22(5): 2841-2851.
[30] Zhang Y, Zhou Y, Zhang L, et al. Electrical treeing behaviors in silicone rubber under an impulse voltage considering high temperature[J]. Plasma Science and Technology, 2018, 20(5): 054012.